LETTER Communicated by John Rinzel

Network Stability from Activity-Dependent Regulation of Neuronal Conductances

Jorge Golowasch
Michael Casey
L. F. Abbott
Eve Marder
Volen Center and Department of Biology, Brandeis University, Waltham, MA 02454-9110, U.S.A.

Activity-dependent plasticity appears to play an important role in the modification of neurons and neural circuits that occurs during development and learning. Plasticity is also essential for the maintenance of stable patterns of activity in the face of variable environmental and internal conditions. Previous theoretical and experimental results suggest that neurons stabilize their activity by altering the number or characteristics of ion channels to regulate their intrinsic electrical properties. We present both experimental and modeling evidence to show that activity-dependent regulation of conductances, operating at the level of individual neurons, can also stabilize network activity. These results indicate that the stomatogastric ganglion of the crab can generate a characteristic rhythmic pattern of activity in two fundamentally different modes of operation. In one mode, the rhythm is strictly conditional on the presence of neuromodulatory afferents from adjacent ganglia. In the other, it is independent of neuromodulatory input but relies on newly developed intrinsic properties of the component neurons.

1 Introduction

Neurons maintain stable properties over extended periods of time despite ion channel turnover and a variety of perturbations. This suggests that neurons have feedback mechanisms that sense overall levels of activity and guide the maintenance of stable patterns of activity (LeMasson, Marder, & Abbott, 1993; Abbott & LeMasson, 1993; Siegel, Marder, & Abbott, 1994; Liu, Golowasch, Marder, & Abbott, 1998). Activity-dependent regulation of conductances of this form has been found and studied at the level of single neurons in a number of preparations (Alkon, 1984; Franklin, Fickbohm, & Willard, 1992; Turrigiano, Abbott, & Marder, 1994; Linsdell & Moody, 1994, 1995; Hong & Lnenicka, 1995, 1997; Li, Jia, Fields, & Nelson, 1996). Intracellular Ca^{2+} appears to be a major feedback element in conductance regulation, which is consistent with the observation that it is a good indicator of

neuronal activity (Ross, 1989; Bito, Deisseroth, & Tsien, 1997). The presence of activity-dependent mechanism that modify intrinsic membrane conductances of individual neurons has a number of interesting functional implications (LeMasson et al., 1993; Abbott & LeMasson, 1993; Siegel et al., 1994; Liu et al., 1998). Here, we explore the consequences of activity-dependent regulation of cellular conductances for network function and stability. For this purpose, we have implemented activity-dependent regulation of the maximum conductances of ionic currents in a three-neuron network resembling the pyloric circuit of the crustacean stomatogastric ganglion (STG).

The pyloric rhythm of the STG consists of alternating bursts of activity in several motor neurons, including the lateral pyloric (LP), pyloric (PY), and pyloric dilator (PD) neurons. Generation of the pyloric rhythm requires the presence of neuromodulatory substances released from axonal terminals of the stomatogastric nerve (*stn*). If the *stn* is cut or blocked, rhythmic activity slows considerably or ceases. However, if the preparation is maintained over a period of days without *stn* modulatory input, rhythmic activity eventually resumes (Thoby-Brisson & Simmers, 1998; see below). Thus, it appears that prolonged removal of modulatory input alters the configuration of the pyloric circuit, allowing it to operate independently of the modulators that it normally requires. This shift may be caused by the removal of trophic influences of the modulators themselves, as suggested by Thoby-Brisson and Simmers (1998), or it may be a secondary response to the decreased activity caused by the absence of modulators. We explore the second possibility here by constructing a model that reproduces the recovery of rhythmicity in the absence of modulatory input using activity-dependent regulation of conductances.

2 Methods

2.1 Experiments. Adult male *Cancer borealis* crabs obtained from local fishermen were kept at 13°C in artificial seawater tanks. Dissections were performed, and both the *stn* and STG were desheathed (Selverston & Moulins, 1987). Most dissections were performed under sterile conditions in a laminar flow hood. In some experiments, sterile saline + 100 g/ml gentamicin + 0.25 g/ml fungizone (Gibco) was used during dissections and all subsequent steps, and in other experiments only sterile saline was used. Similar results were obtained in both cases. Preparations were either kept at 13–14°C in a temperature-controlled incubator (in normal saline + 100 g/ml gentamicin + 0.25 g/ml fungizone), and then taken to a recording setup where activity was recorded with normal saline superfusion, or kept in continuously running normal saline (∼1 ml/min) at 11–14°C. Normal *C. borealis* saline was (in mM): 440 NaCl, 11 KCl, 26 $MgCl_2$, 13 $CaCl_2$, 12 trizma base, 5 maleic acid, pH 7.4–7.5. Preparations included one commisural ganglion, the unpaired esophageal ganglion, the STG, and all the connecting nerves plus the pyloric motor nerves. Pyloric activity was monitored extra-

cellularly from the motor nerves with pin electrodes insulated around the nerves with Vaseline and connected to a differential amplifier (A-M Systems 1700). Intracellular recordings were made with microelectrodes filled with 0.6 M K_2SO_4 + 20 mM KCl (~40–60 MΩ) and an Axoclamp 2B (Axon Instruments, CA). Action potential conduction along the *stn* was blocked by either transecting it with scissors or placing a Vaseline well containing 750 mM sucrose + 1 μM tetrodotoxin (Sigma) around the desheathed *stn*.

2.2 The Model. To evaluate potential mechanisms underlying the reorganization of rhythmic activity following *stn* block, we use a simplified pyloric circuit model (see Figure 1). In this model, a single AB/PD unit represents the electrically coupled anterior burster (AB) and PD neurons of the pyloric network, and a single model PY neuron represents all of the electrically coupled PY neurons in the STG. The third component of the triphasic pyloric rhythm is represented by a model LP neuron.

Each model neuron consists of two compartments (see Figure 1A). A somatic compartment, with potential V_s, represents the cell body and major neurite and generates slow-wave oscillations and plateaus. An axonal compartment, with potential V_a, represents the spike-initiation zone of the axon and produces action potentials. The two compartments are electrically coupled. Action potentials do not play a particularly significant role in the model we construct, and indeed the pyloric rhythm can be generated by the STG when action potentials are blocked (Raper, 1979). Nevertheless, they are included in the model for added realism.

The somatic compartment of each cell has a membrane capacitance C_s = 0.2 nF, and it contains leakage, Ca^{2+}, K^+, and A-type K^+ membrane conductances, and a proctolin-dependent modulatory conductance (in the AB/PD and LP neurons only). The maximal conductances of these currents (the conductance when the currents are fully activated) are labeled by $\bar{g}_{Ls}$, $\bar{g}_{Ca}$, $\bar{g}_K$, $\bar{g}_A$, and $\bar{g}_{Proc}$. The parameters $\bar{g}_{Ls}$, $\bar{g}_A$, and $\bar{g}_{Proc}$ are fixed, and their values for the three different cell types used in the network model are listed in Table 1. The other two maximal conductances in the somatic compartment, $\bar{g}_{Ca}$ and $\bar{g}_K$, are dynamic variables subject to activity-dependent modification. The equations that determine their values are given below.

The proctolin conductance is included to model the effects of neuromodulators released by *stn* axons. The peptide proctolin is only one of many substances released from axon terminals of the *stn*, but it is a particularly potent modulator of the pyloric rhythm (Hooper & Marder, 1987; Nusbaum & Marder, 1989a,b). Proctolin produces an inward current in the AB and LP neurons at physiological membrane potentials, and the membrane conductance it activates in the LP neuron has been measured and described mathematically (Golowasch & Marder, 1992; Golowasch, Buchholtz, Epstein, & Marder, 1992). For the results shown in Figures 3 and 4, the proctolin conductance is activated, but it is turned off in Figure 5 to simulate blockade of the *stn*.

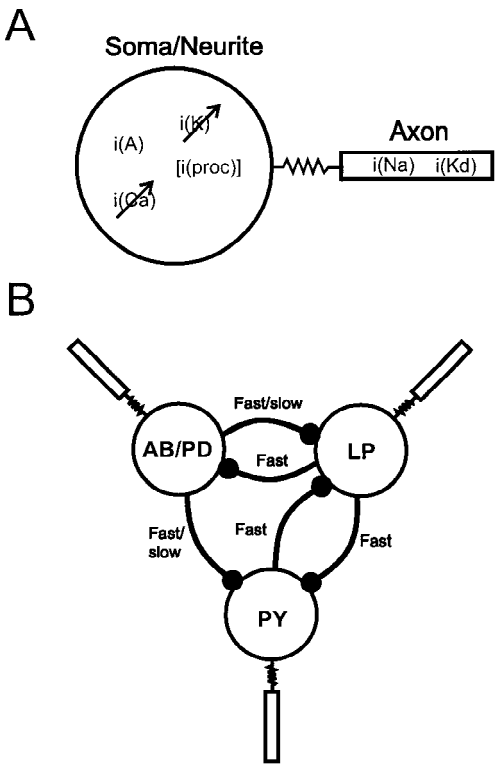

Figure 1: Model pyloric network. (A) Each model neuron has two components, one representing the soma and primary neurite and containing an unregulated A-type K^+ current, $i(A)$, regulated K^+ and Ca^{2+} currents, $i(K)$ and $i(Ca)$, and a modulatory proctolin current, $i(proc)$ (in AB/PD and LP neurons, but not in the PY neuron). The axon compartment contains fast Na^+ and delayed rectifier K^+ currents, $i(Na)$ and $i(Kd)$. (B) The synaptic connectivity of the circuit model. Filled circles denote inhibitory connections. Synapses from the AB/PD unit have both fast and slow components, while all other synapses are fast.

The somatic compartment also contains synaptic conductances reflecting connections to other neurons. The synaptic conductances used to construct the model circuit are described below; for now we use I_{syn} to represent the total synaptic current. The basic equation for the somatic compartment is

$$C_S\frac{dV_s}{dt} = -I_{syn}-\bar{g}_{Ls}(V_s-E_L)-\bar{g}_{Ca}m_{Ca}^3h_{Ca}(V_s-E_{Ca})-\bar{g}_K m_K^4(V_s-E_K)$$
$$-\bar{g}_A m_A^3 h_A(V_s-E_K)-\bar{g}_{Proc}m_{proc}(V_s-E_{proc})-\bar{g}_E(V_s-V_a). \qquad (2.1)$$

Table 1: Values of Maximal Conductance Parameters for the Somatic and Axonal Compartments of All Three Model Neurons (in μS).

Variable	AB/PD	LP	PY
$\bar{g}_{Ls}$	0.03	0.025	0.015
$\bar{g}_{A}$	0.45	0.1	0.25
$\bar{g}_{Proc}$	0.006	0.008	0
$\bar{g}_{E}$	0.01	0.01	0.01
$\bar{g}_{La}$	0.0075	0.0075	0.0075
$\bar{g}_{Na}$	0.3	0.3	0.3
$\bar{g}_{Kd}$	4	4	4

Note: The dynamically regulated maximal conductances for the Ca^{2+} and K^+ currents are described in the text.

The parameters $E_L = -68$ mV, $E_{Ca} = 120$ mV, $E_K = -80$ mV, and $E_{proc} = -10$ mV are the reversal potentials for the different conductances. The last term in this equation represents the coupling between the somatic and axonal compartments, and the value of the intercompartmental conductance $\bar{g}_E$ is given in Table 1.

The axonal compartment has a capacitance $C_a = 0.02$ nF, and it contains leakage, Na^+ and delayed rectifier K^+ conductances, and the conductance due to the coupling to the somatic compartment. The maximal conductance of the leakage current for the axonal compartment is labeled $\bar{g}_{La}$, and the Na^+ current has maximal conductance $\bar{g}_{Na}$. The K^+ conductance for the axonal compartment is different from the K^+ conductance in the somatic compartment. It is a delayed rectifier conductance, and its maximal conductance parameter is labeled $\bar{g}_{Kd}$. All of the maximal conductance parameters in the axonal compartment take fixed values (i.e., they are not subject to activity-dependent regulation), and these are given in Table 1. The basic equation governing the membrane potential of the axonal compartment is

$$C_a \frac{dV_a}{dt} = -\bar{g}_{La}(V_a - E_L) - \bar{g}_{Na} m_{Na}^3 h_{Na}(V_a - E_{Na}) - \bar{g}_{Kd} m_{Kd}^4 (V_a - E_K) - \bar{g}_E (V_a - V_s), \tag{2.2}$$

with the reversal potentials $E_{Na} = 20$ mV, $E_K = -80$ mV, and $E_L = -68$ mV.

The variables m_{Ca}, h_{Ca}, m_K, m_A, h_A, m_{proc}, m_{Na}, h_{Na}, and m_{Kd} appearing in equations 2.1 and 2.2 are gating variables determined by the usual Hodgkin-Huxley equations (with subscripts dropped),

$$\tau_m(V)\frac{dm}{dt} = m_\infty(V) - m \quad \text{or} \quad \tau_h(V)\frac{dh}{dt} = h_\infty(V) - h \tag{2.3}$$

Table 2: Values of Parameters for the Functions in the Hodgkin-Huxley Equations for the Gating Variables.

Variable	m_∞ or h_∞		τ_m or τ_h			
	$V_{1/2}$ (mV)	s (1/mV)	$V_{1/2}$ (mV)	s (1/mV)	A (ms)	B (ms)
m_{Ca}	−61.2	0.205	−65	0.2	30	−5
h_{Ca}	−75	−0.15	—	—	150	0
m_K	−35	0.1	−54	−0.125	2	55
m_A	−60	0.2	—	—	0.1	0
h_A	−68	−0.18	—	—	50	0
m_{proc}	−55	0.2	—	—	6	0
m_{Na}	−42.5	0.1	—	—	0.025	0
h_{Na}	−50	−0.13	−77	0.12	0	10
m_{Kd}	−41	0.2	58	−0.05	12.2	10.5

with

$$m_\infty(V) \quad \text{or} \quad h_\infty(V) = \frac{1}{1+\exp[s(V_{1/2}-V)]} \tag{2.4}$$

and

$$\tau_m(V) \quad \text{or} \quad \tau_h(V) = A + \frac{B}{1+\exp[s(V_{1/2}-V)]}\,. \tag{2.5}$$

The values of the parameters appearing in these equations for the different gating variables are given in Table 2.

The maximal conductances for most of the membrane currents in our model, like those in all conventional neuron models, are described by fixed parameters (those given in Table 1). However, the maximal conductances of the Ca^{2+} and K^+ currents in the somatic compartments are not fixed; instead, they are dynamic variables affected by the Ca^{2+} influx through the Ca^{2+} current $I_{Ca} = \bar{g}_{Ca} m_{Ca}^3 h_{Ca}(V_s - E_{Ca})$. This is how we model activity-dependent regulation of neuron conductances. We include only two activity-regulated currents to keep the model relatively simple. As in previous models (LeMasson et al., 1993; Abbott & LeMasson, 1993; Siegel et al., 1994; Liu et al., 1998), we allow Ca^{2+} influx to modify the maximal conductances at a slow rate. The activity-dependent regulation of the maximum conductances $\bar{g}_{Ca}$ and $\bar{g}_K$ is mediated by a dynamic variable z (Abbott & LeMasson, 1993) by writing

$$\bar{g}_{Ca} = \frac{G_{Ca}}{2}[1+\tanh(z)] \quad \text{and} \quad \bar{g}_K = \frac{G_K}{2}[1-\tanh(z)]. \tag{2.6}$$

Note that these equations constrain the sum of the maximal conductances to a constant value, $g_{Ca}+g_K = (G_{Ca}+G_K)/2$. The fixed parameters $G_{Ca} = 0.2\,\mu$S

and $G_K = 16\ \mu$S determine the range over which g_{Ca} and g_K can vary. The value of z is then governed by the relationship between I_{Ca} and a target or equilibrium value (a fixed parameter),

$$\tau_z \frac{dz}{dt} = \tanh(I_{target} - I_{Ca}), \tag{2.7}$$

with $\tau_z = 5$ s to ensure that conductance regulation is slower than any of the other processes affecting the dynamics of the model neurons. In the biological neurons, we expect activity-dependent conductance regulation to be even slower, taking hours or even days. Although the model of conductance regulation we are using is closely related to a previous model (Abbott & LeMasson, 1993), there are some differences. The most significant of these is the absence of a term $-z$ on the right side of equation 2.7. Making the right side of equation 2.7 independent of z gives the model much more flexibility in finding stable configurations (Liu et al., 1998). Other changes are the use of the Ca^{2+} current rather than Ca^{2+} concentration as a measure of activity, and the imposition of equation 2.6 as a constraint rather than as a consequence of the dynamics of the model. These changes are less significant.

The target current I_{target} is a fixed parameter that represents the level of Ca^{2+} influx at which all the Ca^{2+}-dependent processes that change the Ca^{2+} and K^+ conductances come to equilibrium. When $I_{Ca} < I_{target}$, indicating low average levels of activity, the maximal conductance of the inward Ca^{2+} current in the model increases and that of the outward K^+ current decreases. When $I_{Ca} > I_{target}$, reflecting high activity levels, the Ca^{2+} conductance decreases and the K^+ conductance increases. Because Ca^{2+} influx is correlated with activity (LeMasson et al., 1993; Ross, 1989; Bito et al., 1997), the Ca^{2+} dependence of the maximal conductances $\bar{g}_{Ca}$ and $\bar{g}_K$ provides a feedback loop allowing changes of electrical activity to modify intrinsic properties (LeMasson et al., 1993; Abbott & LeMasson, 1993; Siegel et al., 1994; Liu et al., 1998). The steady-state pattern of activity that a given model neuron exhibits is controlled by the value of I_{target}. We use the Ca^{2+} current directly in this model, rather than a computed intracellular Ca^{2+} concentration, because the Ca^{2+} concentration near the cell membrane, where many signal transduction pathways are likely to originate, is roughly proportional to the Ca^{2+} current. We allow each neuron type to have a different I_{target}. This is based on an assumption that the developmental determination of neuronal identity sets a neuron's characteristic target level and that, once set, this becomes a determinant of the neuron's electrical properties. Although we use Ca^{2+} as the messenger that conveys a signal related to activity to the interior of the cell, virtually any other activity-dependent second messenger pathway could be used.

In our circuit model, we used the values $I_{target} = 0.4$ nA for the AB/PD unit, $I_{target} = 0.3$ nA for the LP neuron, and $I_{target} = 0.5$ nA for the PY cell. These values were obtained by first adjusting the parameters for each neu-

ron until a pattern of activity resembling the pyloric rhythm was generated. Then the time average value of I_{Ca} was computed in each neuron, and this was used as the value of I_{target} for that cell. The activity of the network was not particularly sensitive to the precise values of I_{target} used. A reasonable pattern of rhythmic activity could be obtained over a range of target values. However, substantially different values produce modified activity patterns, such as the absence of rhythmic activity, or unrealistic intrinsic activities when the neurons are isolated (for example, all the neurons acting as intrinsic bursters).

Figure 1B shows the synaptic connections used in the model to simulate the configuration of the pyloric circuit. The synaptic strengths and dynamics are based on experimental results (Marder & Eisen, 1984), but are simplified in the model. The synaptic currents are expressed as graded functions of the presynaptic membrane potential, and they fall into fast and slow classes. All the synapses from the LP and PY neurons are fast, and we model these as instantaneous functions of the presynaptic membrane potential. The synapses made by the AB/PD neuron have both fast and slow components to match the fast and slow inhibitory postsynaptic potentials evoked by activity in the AB and PD neurons of the STG (Marder & Eisen, 1984).

The synaptic currents depend on the membrane potentials of the pre- and postsynaptic somatic compartments, which we label V_s^{pre} and V_s^{post}. The dependence is on the presynaptic potential in the somatic compartment because the connections among neurons within the STG arise from the principal neurite connected to the soma, not from the axon. For all of the fast synapses coming from the LP and PY neurons, the postsynaptic current is $I_{syn} = I_{fast}$, where

$$I_{fast} = \frac{\bar{g}_{fast}\left(V_s^{post} - E_{syn}\right)}{1 + \exp[s_{fast}(V_{fast} - V_s^{pre})]} \tag{2.8}$$

with $s_{fast} = 0.2/\text{mV}$ and $V_{fast} = -50$ mV. For synapses arising from the AB/PD unit, the postsynaptic current is $I_{syn} = I_{fast} + I_{slow}$ with I_{fast} given as above and

$$I_{slow} = \bar{g}_{slow} m_{slow}(V_s^{post} - E_{syn}) \tag{2.9}$$

with

$$\frac{dm_{slow}}{dt} = \frac{k_1(1 - m_{slow})}{1 + \exp[s_{slow}(V_{slow} - V_s^{pre})]} - k_2 m_{slow}, \tag{2.10}$$

where $s_{slow} = 1/\text{mV}$ and $V_{slow} = -55$ mV. For both fast and slow synaptic currents, the reversal potential is $E_{syn} = -75$ mV. The maximal synaptic conductances for the fast synapses, $\bar{g}_{fast}$, are given in Table 3, and the values for the slow synapses, $\bar{g}_{slow}$, are in Table 4.

Table 3: Values of Maximal Conductances $\bar{g}_{fast}$ for the Fast Synapses from the LP and PY Neurons and the Fast Component of synapses from the AB/PD (in μS).

Post/Pre	From AB/PD	From LP	From PY
To AB/PD	—	0.01	0
To LP	0.015	—	0.005
To PY	0.005	0.02	—

Note: Presynaptic neurons are labeled in the columns and the postsynaptic neurons in the rows.

Table 4: Values of Maximal Conductances and Kinetic Parameters for the Slow Component of Synapses arising from the AB/PD.

Post	$\bar{g}_{slow}$ (μS)	k_1 (1/ms)	k_2 (1/ms)
To LP	0.025	1	0.03
To PY	0.015	1	0.008

3 Results

3.1 Block of the *stn* and Recovery of the Pyloric Rhythm. Figure 2 shows experimental results on the effect of blocking the *stn* and the eventual recovery of the pyloric rhythm. Before blockade of the *stn*, the preparation shown in Figure 2A displayed a robust pyloric rhythm. Immediately following blockade of action potential conduction along the *stn*, the rhythm completely terminated. However, when the block was maintained for approximately 24 hours, rhythmic pyloric activity resumed. The results in Figure 2A are typical for preparations that survive for 24 hours or more in organ culture. The average control pyloric frequency before blockade for all preparations was 1.14 ± 0.09 Hz, and this fell to 0.01 ± 0.01 Hz immediately after the *stn* block (see Figure 2B). Rhythmic pyloric activity resumed in 24 hours and achieved an average frequency of 0.37 ± 0.10 Hz after 48 hours (see Figure 2B). The frequency of the pyloric rhythm after recovery was significantly slower than in acute *in vitro* preparations with the *stn* intact, but similar to the pyloric frequency *in vivo* for unfed animals. In unpublished results of R. Zarum, P. Meyrand, and E. Marder, the pyloric frequency in unfed animals ($n = 5$) was 0.26 ± 0.23 Hz during the day and 0.50 ± 0.16 Hz at night, while in feeding animals ($n = 4$) it was 0.80 ± 0.15 Hz during the day and 1.03 ± 0.19 Hz at night.

3.2 Self-Assembly of a Pyloric Circuit. A novel feature of models with activity-dependent maximal conductances is that they can self-assemble the conductances needed to achieve a particular pattern of activity (Liu et al,

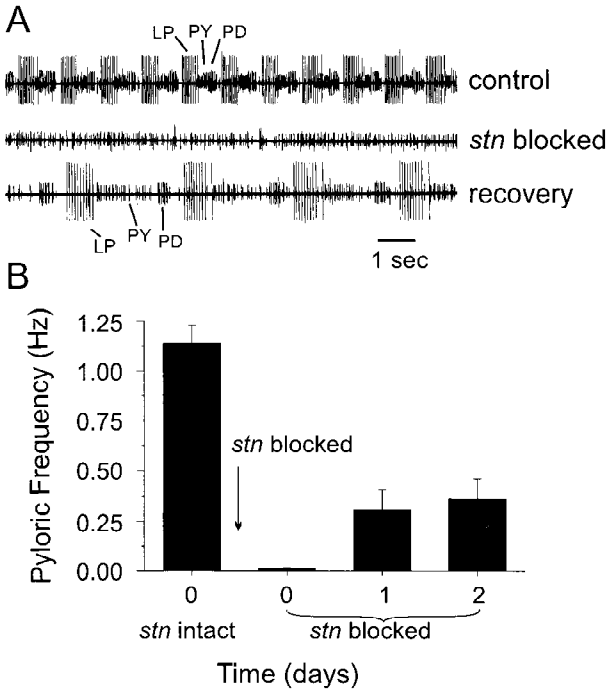

Figure 2: Effect of *stn* block on the pyloric rhythm. (A) Extracellular recordings from the lateral ventricular nerve (*lvn*). The LP neuron action potentials are the largest spikes, those of the PD neuron appear as medium-amplitude spikes, and the small spikes correspond to the PY neurons. Top trace: Recordings before *stn* block (control) show a robust pyloric rhythm with a frequency of 0.88 Hz. Middle trace: After block of action potential conduction along the *stn*, the pyloric rhythm is completely suppressed and the PD and LP neurons are inactive. Bottom trace: After 22 hours of recovery time (in normal saline at 12°C) the pyloric rhythm is present (recovery) at a lower frequency than control (0.31 Hz). (B) Histogram of the pyloric frequency before and at different times after *stn* block. The frequency of the pyloric rhythm drops from 1.14 ± 0.09 Hz ($n = 28$) to 0.01 ± 0.01 Hz, ($n = 27$) immediately after the *stn* is blocked. It then recovers to 0.31 ± 0.10 Hz ($n = 13$) after 24 hours and to 0.37 ± 0.10 Hz ($n = 7$) after 48 hours. Differences between these groups are statistically significant (ANOVA on ranks, $F(3, 16) = 10.671$, $P < 0.001$).

1998). The individual model AB/PD, LP, and PY neurons we use here also display this feature. Figure 3A shows the activity of the three model neurons after the Ca^{2+}-dependent regulation scheme has achieved steady-state values for the maximal conductances of the Ca^{2+} and K^+ currents when the

neurons are isolated from each other. In this condition, the AB/PD and LP neurons fire in bursts, and the PY neuron fires action potentials tonically. Immediately after the synaptic connections of the circuit model shown in Figure 1B are turned on, these activity patterns change (see Figure 3B). These changes activate the dynamical regulation of $\bar{g}_{Ca}$ and $\bar{g}_K$ by making the Ca^{2+} currents deviate from the target levels I_{target}. Ultimately a new equilibrium configuration is established with an activity pattern similar to that of the pyloric rhythm of the STG (see Figure 3C). With the synaptic connections in place and the activity-dependent conductances at equilibrium values, a stable triphasic rhythm results from the coordinated effects of synaptic and intrinsic membrane conductances. Generation of the pyloric rhythm is accompanied by a change in the intrinsic properties of the neurons. The changes in the intrinsic properties of the individual neurons brought about by connecting the neurons synaptically into a circuit can be seen by comparing Figures 3A and 3D. The activity of the neurons immediately after they are uncoupled (see Figure 3D) is different from their steady-state activity after they have been uncoupled for a long period of time (see Figure 3A). The LP neuron no longer bursts but fires action potentials tonically, and PY fires action potentials tonically at a higher rate than at steady state. AB/PD show little change compared to steady state.

The model circuit can self-assemble and produce triphasic rhythmic activity from any initial configuration of Ca^{2+} and K^+ conductances in the three neurons. The activity-dependent conductances in the circuit are specified by the values of the z variables for each of the three neurons. We have studied how these variables evolve as a function of time. There is a single stable fixed point representing the activity seen in Figure 3C, and no obstructions prevent any initial set of z values from ultimately ending up at the fixed point. The three-dimensional map of z flows is rather confusing to view, so we illustrate its basic features in a simpler manner in Figure 4 by showing self-assembly from two different initial configurations. In Figure 4A, the two initial configurations show different patterns of activity, but both converge to identical three-phase rhythms in the steady state. Figure 4B shows the temporal evolution of the Ca^{2+} and K^+ conductances for these two cases, indicating that the same final maximal conductances are achieved starting from different initial values.

3.3 Recovery from Modulatory Blockade. Figure 5 compares the behavior of the model with experimental results on the effect of *stn* block and the recovery of rhythmic activity. Initially the activity of the model network with the proctolin current activated (see Figure 5A, left) matches the pyloric activity of the experimental preparation with the *stn* intact (see Figure 5A, right). The same AB/PD-LP-PY sequence of bursting activity, with a silent gap between AB/PD and LP phases, is produced by both networks. To simulate the effects of blocking the *stn*, we set the proctolin conductance in the LP and AB/PD neurons to zero (see Figure 5B, left). This immediately

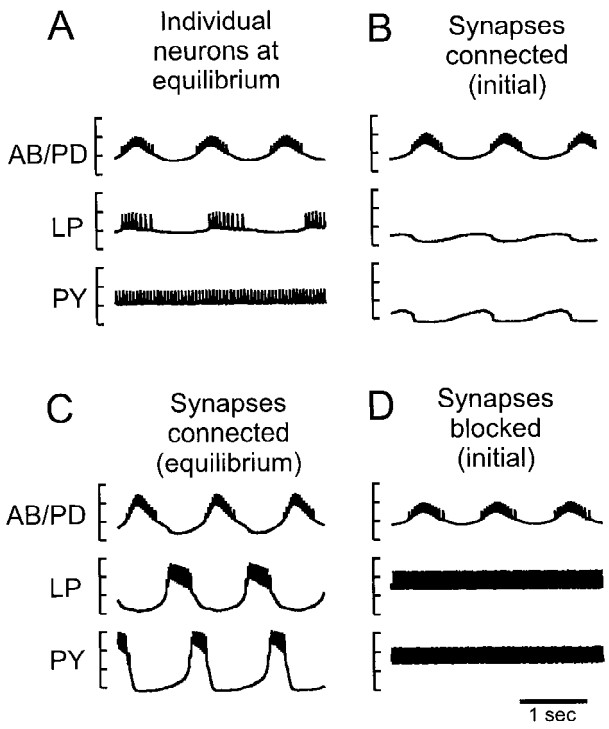

Figure 3: Activity of the model pyloric network. The tick marks on each vertical scale indicate 10 mV, the lowest being −60 mV. (A) Activity of the individual neurons at equilibrium when uncoupled. (B) Activity of the network immediately after turning on the synaptic connections. (C) Activity of the synaptically connected network at steady state after activity-dependent conductances have come to equilibrium. (D) Activity of the individual model neurons immediately after turning off the synaptic connections. The difference in the activity compared to A is a reflection of activity-dependent regulation of conductances that occurs during long-term synaptic coupling.

terminates the rhythmic activity of the model network, duplicating the effect of blocking the *stn* in the real preparation (see Figure 5B, right). The suppression of the rhythm following the elimination of the proctolin conductance reduces I_{Ca}, causing a slow up-regulation of Ca^{2+} conductances and down-regulation of K^+ conductances. This enhances bursting activity in the AB/PD neuron and strengthens the ability of the LP neuron to rebound following synaptic inhibition. Restoration of the pyloric rhythm in the model network after elimination of the proctolin conductance (see Figure 5C, left) matches the natural resumption of the rhythm (see Figure 5C,

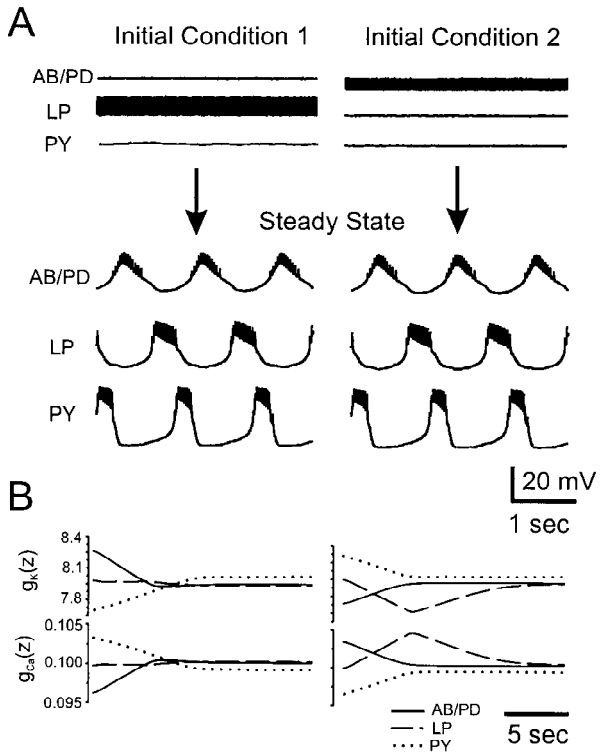

Figure 4: Self-assembly of the model pyloric network. (A) Top panels: Firing characteristics of the model network for two different initial conditions. Traces for AB/PD, LP, and PY units are indicated. Bottom panels: Steady-state condition reached by the network. The final state is the same for both runs. (B) Top panels: Temporal evolution of the maximal conductance $\bar{g}_K$ for each of the three neurons in the network. Bottom panels: Evolution of the maximal conductance $\bar{g}_{Ca}$. The conductance change is nonmonotonic for some of the cells, but the same final values are achieved for both sets of initial conditions. Units for the maximal conductances are μS.

right) after *stn* block and, like it, produces a slower rhythm than under control conditions.

4 Discussion

The nervous system must continuously balance two apparently opposing forces. While it is critical for neurons and synapses to be plastic, it is equally important that the functional characteristics of a given network be preserved

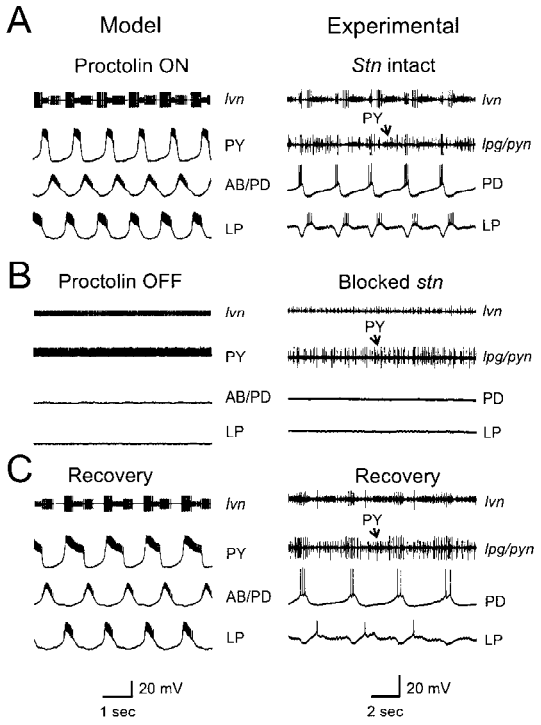

Figure 5: Effect of *stn* block on the model and biological pyloric networks. Experiments were as described in Figure 1 except that intracellular recordings of the PD and LP neurons were made before, immediately after, and 24 hours after *stn* block. Microelectrodes were withdrawn after recording with the *stn* blocked (B) and the cells were reimpaled the following day (C). Experimental results (right) show extracellular recordings of two motor nerves, *lvn* and *lpg/pyn*, and intracellular recordings of the PD (also midsize unit on the *lvn*) and LP (also largest unit on the *lvn*) neurons. PY neuron activity appears as the small unit on the *lvn* and *lpg/pyn* recordings (arrow). Model results (left) simulate extracellular recordings of the *lvn* and intracellular recordings of the PY, AB/PD, and LP neurons. (A) In control conditions (proctolin conductance activated in the model and *stn* intact in the experimental preparation), both model and experimental traces show the triphasic pyloric rhythm. (B) Left: Activity of the model network immediately after the proctolin conductance was set to zero. The PY neuron remains depolarized and fires action potentials tonically at high frequency while AB/PD and LP neurons are silent. Right: When the *stn* was blocked, the PY units (recorded extracellularly on the *lpg/pyn* and *lvn*) showed high-frequency tonic firing while the LP and PD neurons were silent. (C) Left: Recovery of pyloric activity in the model following prolonged removal of the proctolin current. Right: Recovery of activity in the biological network after prolonged block of the *stn*.

(Marder, 1998). How do networks retain their functional stability despite the many short- and long-term mechanisms that dramatically alter neuronal and synaptic properties? In previous work, we have proposed models that maintain stable activity of single neurons through homeostatic regulation of membrane currents (Abbott & LeMasson, 1993; LeMasson et al., 1993; Siegel et al., 1994; Liu et al., 1998). We now suggest that activity-dependent processes acting at the single-neuron level can stabilize network activity as well. Thus, at both the single-neuron and network level, plasticity, which is normally considered an agent for change, can have a stabilizing influence.

In the simple model presented here, stable network function is maintained because each neuron modifies its intrinsic properties in response to changes in its own activity. We constructed the model in such a way that a locally stable configuration corresponding to rhythmic activity existed. However, it was not obvious that this configuration would be unique or that it could act as an attractor for a wide variety of initial network configurations. The uniqueness of the steady-state activity pattern exhibited by the model is primarily due to the fact that the neurons had a small number of conductances that were highly constrained. More complex single-neuron models with dynamically regulated conductances do not display unique steady-state configurations (Liu et al., 1998). In more complex models, it will probably be quite difficult to ensure that the desired pattern of activity is reached from a wide variety of initial states. This may require more numerous and elaborate feedback schemes (Liu et al., 1998) and some restrictions on the allowed initial configurations.

Our results and those of Thoby-Brisson and Simmers (1998) show that the pyloric rhythm can be produced by two qualitatively different mechanisms. In one mode, rhythmic activity depends on the release of modulatory substances that activate membrane currents in specific target neurons. In the second mode, rhythmic activity is independent of modulatory substances. The transition from the former to the latter in our model occurs as a result of changes in the intrinsic properties of pyloric network neurons. The model makes the experimentally testable prediction that there should be significant alterations in membrane currents as the ganglion resumes rhythmic activity following *stn* blockade.

The perturbation used in these experiments and those of Thoby-Brisson and Simmers (1998) is quite extreme. However, we suggest that the same mechanisms that are called into play by these severe manipulations are used throughout the lifetime of the animal to maintain stable network activity. From this point of view, it is interesting that the pyloric rhythm subsequent to *stn* blockade has a similar period as that in unfed animals. In the wild, we expect that much of the animal's time is spent in the unfed state, so this may reflect the long-term mean activity level of the *in vivo* pyloric network. The "control" condition in the experiments we report, with anterior modulatory projection neurons left attached, may produce unphysiologically elevated activity levels because pathways from the brain and other

parts of the nervous system, which may suppress activity in the modulatory projection neurons, have been removed during the dissection. The fact that the pyloric rhythm after recovery is significantly slower than in the "control" conditions may reflect the fact that the network is self-regulating to the characteristic frequency of an unfed animal.

The basic biological phenomenon presented both here and in Thoby-Brisson and Simmers (1998) is that removal of modulatory inputs, with consequent loss of activity, is followed, after a significant period of time, by a restoration of activity that no longer depends on modulatory inputs. The change in the network brought about by prolonged blockade of modulatory inputs may be either a direct or an indirect consequence of the absence of modulatory substances. In our model, the effect is indirect because intrinsic conductance regulation is a response to changes in network activity brought about by the absence of modulators. The network model demonstrates that such a mechanism is sufficient to account for our experimental results. Thoby-Brisson and Simmers (1998) have argued in favor of a direct effect of the removal of modulators that is independent of activity. In support of this hypothesis, they found that depolarization of the preparation with high K^+ or through activation by muscarinic agonists did not prevent the resumption of activity following blockade of modulatory inputs. However, interpretation of their results is confounded by the fact that the pyloric frequencies shown for those two treatments were substantially slower than those with anterior inputs intact, and in fact slower than at the end of the treatments. Therefore, the treatments may have provided insufficient excitation to prevent activity-dependent regulation processes from occurring. In comparing our experimental results and those of Thoby-Brisson and Simmers (1998), it should be kept in mind that they involved different species that showed significant differences in the time course of rhythm restoration. While our modeling results argue that a simple activity-dependent mechanism could account for the rhythm restoration phenomenon, untangling the relative contributions of activity and neuromodulators acting trophically will require further experimental work.

Although we allowed the intrinsic properties of the neurons in our model to vary with activity, we kept the synaptic strengths within the network fixed. Further experimental work is required to determine if the synaptic strengths in the control and recovered networks are significantly different. It is interesting that restoration of rhythmic activity in the model network did not require any synaptic plasticity, but could occur solely through regulation of intrinsic conductances. Nevertheless, activity-dependent changes in synaptic efficacy are undoubtedly a major mechanism for network plasticity (Bliss & Collingridge, 1993; Artola & Singer, 1993; Malenka & Nicoll, 1993). Recent work suggests that homeostatic mechanisms may play a role in determining synaptic strength (Turrigiano, Leslie, Desai, Rutherford, & Nelson, 1998; Davis & Goodman, 1998). A full understanding of network stability will require an analysis of the interactions between synaptic and

intrinsic plasticity, including both homeostatic and nonhomeostatic mechanisms.

Acknowledgments

Our work was supported by MH 46742, the W. M. Keck Foundation, and the Sloan Center for Theoretical Neurobiology at Brandeis University.

References

Abbott, L. F., & LeMasson, G. (1993). Analysis of neuron models with dynamically regulated conductances. *Neural Comp., 5*, 823–842.

Alkon, D. L. (1984). Calcium-mediated reduction of ionic currents: A biophysical memory trace. *Science, 226*, 1037–1045.

Artola, A., & Singer, W. (1993). Long-term depression of excitatory synaptic transmission and its relationship to long-term potentiation. *Trends Neurosci., 16*, 480–487.

Bito, H., Deisseroth, K., & Tsien, R. W. (1997). Ca^{2+}-dependent regulation in neuronal gene expression. *Curr. Opin. Neurobiol., 7*, 419–429.

Bliss, T. V. P., & Collingridge, G. L. (1993). A synaptic model of memory: Long-term potentiation in the hippocampus. *Nature, 361*, 31–39.

Davis, G. W., & Goodman, C. S. (1998). Genetic analysis of synaptic development and plasticity: Homeostatic regulation of synaptic efficacy. *Curr. Opin. Neurobiol., 8*, 149–156.

Franklin, J. L., Fickbohm, D. J., & Willard, A. L. (1992). Long-term regulation of neuronal calcium currents by prolonged changes of membrane potential. *J. Neurosci., 12*, 1726–1735.

Golowasch, J., Buchholtz, F., Epstein, I. R., & Marder, E. (1992). Contribution of individual ionic currents to activity of a model stomatogastric ganglion neuron. *J. Neurophysiol., 67*, 341–349.

Golowasch, J., & Marder, E. (1992). Proctolin activates an inward current whose voltage dependence is modified by extracellular Ca^{2+}. *J. Neurosci., 12*, 810–817.

Hong, S. J., Lnenicka, G. A. (1995). Activity-dependent reduction in voltage-dependent calcium current in a crayfish motoneuron. *J. Neurosci., 15*, 3539–3547.

Hong, S. J., & Lnenicka, G. A. (1997). Characterization of a P-type calcium current in a crayfish motoneuron and its selective modulation by impulse activity. *J. Neurophysiol., 778*, 76–85.

Hooper, S. L., & Marder, E. (1987). Modulation of the lobster pyloric rhythm by the peptide proctolin. *J. Neurosci., 7*, 2097–2112.

LeMasson, G., Marder, E., & Abbott, L. F. (1993). Activity-dependent regulation of conductances in model neurons. *Science, 259*, 1915–1917.

Li, M., Jia, M., Fields, R. D., & Nelson, P. G. (1996). Modulation of calcium currents by electrical activity. *J. Neurophysiol., 76*, 2595–2607.

Linsdell, P., & Moody, W. J. (1994). Na^+ channel mis-expression accelerates K^+ channel development in embryonic *Xenopus laevis* skeletal muscle. *J. Physiol. (London), 480*, 405–410.

Linsdell, P., & Moody, W. J. (1995). Electrical activity and calcium influx regulate ion channel development in embryonic *Xenopus* skeletal muscle. *J. Neurosci., 15*, 4507–4514.

Liu, Z., Golowasch, J., Marder, E., & Abbott, L. F. (1998). A model neuron with activity-dependent conductances regulated by multiple calcium sensors. *J. Neurosci., 18*, 2309–2320.

Malenka, R. C., & Nicoll, R. A. (1993). NMDA-receptor-dependent synaptic plasticity: Multiple forms and mechanisms. *Trends Neurosci., 16*, 521–527.

Marder, E. (1998). From biophysics to models of network function. *Annu. Rev. Neurosci., 21*, 25–45.

Marder, E., & Eisen, J. S. (1984). Transmitter identification of pyloric neurons: Electrically coupled neurons use different transmitters. *J. Neurophysiol., 51*, 1345–1361.

Nusbaum, M. P., & Marder, E. (1989a). A modulatory proctolin-containing neuron (MPN). I. Identification and characterization. *J. Neurosci., 9*, 1591–1599.

Nusbaum, M. P., & Marder, E. (1989b). A modulatory proctolin-containing neuron (MPN). II. State-dependent modulation of rhythmic motor activity. *J. Neurosci., 9*, 1600–1607.

Raper, J. A. (1979). Non-impulse mediated synaptic transmission during the generation of a cyclic motor program. *Science, 205*, 304–306.

Ross, W. M. (1989). Changes in intracellular calcium during neuron activity. *Annu. Rev. Physiol., 51*, 491–506.

Selverston, A. I., & Moulins, M. (Eds.). (1987). *The crustacean stomatogastric system*. New York: Springer-Verlag.

Siegel, M., Marder, E., & Abbott, L. F. (1994). Activity-dependent current distributions in model neurons. *Proc. Natl. Acad. Sci. USA, 91*, 11308–11312.

Thoby-Brisson, M., & Simmers, J. (1998). Neuromodulatory inputs maintain a lobster motor pattern-generating network in a modulation-dependent state: Evidence from long-term decentralization *in vivo*. *J. Neurosci., 18*, 2212–2225.

Turrigiano, G., Abbott, L. F., & Marder, E. (1994). Activity-dependent changes in the intrinsic properties of cultured neurons. *Science, 264*, 974–977.

Turrigiano, G., Leslie, K. R., Desai, N. S., Rutherford, L. C., & Nelson, S. B. (1998). Activity-dependent scaling of quantal amplitude in neocortical neurons. *Nature, 391*, 892–896.

Received May 13, 1998; accepted September 11, 1998.